AIAA JOURNAL
Vol. 43, No. 6, June 2005

Turbulent Flow Downstream of a Propeller, Part 1: Wake Turbulence

Denis A. Lynch III* and William K. Blake†
U.S. Naval Surface Warfare Center, West Bethesda, Maryland 20817-5700
and
Thomas J. Mueller‡
University of Notre Dame, Notre Dame, Indiana 46556-5684

To examine the aeroacoustic response of the downstream blade row of a rotor/stator pair, the turbulent flowfield between the two components must be accurately represented. To that end, a recent experimental study sought to examine this complex flowfield, establishing a causal relationship between the flowfield influences and their relative contributions to the total turbulence. Although these influences and their relative impact might depend on specific geometry, two will play a dominant role in almost every rotor/stator application: wake turbulence from the upstream blade row (the topic of Part 1) and turbulence ingested by the system and modified by the upstream blade row (the topic of Part 2). The extensive scope of decomposing these influences necessitates their discussion in seperate publications. Part 1 begins with an overview as to the relevence and utility of separating these influences, providing motivation for the study. The paper then examines the contribution of the broadband and tonal contributions associated with wake turbulence. A model is proposed that infers broadband turbulence levels from a single, appropriately chosen length scale. This length scale is determined through reconstruction of the temporal mean wake profile shape utilizing the tonal component of the ensemble-averaged, measured wake spectra. Results show that simple models can be used effectively to isolate the wake turbulence contribution, forwarding the concept of a globally applicable theory for use in modeling efforts involving similar flowfields. Part 2 examines turbulence ingested by the system and modified by the upstream upstream blade row. A theoretical model is adapted to predict the level of ingested turbulence suppression using easily quantified geometric arguments. With an appropriate choice of coordinate system, this model accurately predicts broadband suppression of ingested turbulence, showing that simple models can be used to isolate contributions and forwarding the concept of a globally applicable theory for extracting such information from other similar flowfields.

Nomenclature

B	=	number of propeller blades
D	=	propeller diameter
f	=	temporal frequency
i_{wake}	=	quantity specifically dealing with propeller wake
$i_1 = i_x$	=	quantity i in the freestream direction
i_2	=	quantity i in the direction normal to airfoil (stator) surface
i_3	=	quantity i in the spanwise direction of airfoil (stator) surface
i_∞	=	freestream quantity
J	=	propeller advance ratio
k	=	wave number
n	=	propeller rotation rate, rev/s
p	=	wake exponential shape factor
R	=	radial distance from propeller centerline
R_{tip}	=	radial distance of propeller tip from propeller centerline
U	=	mean velocity component
U_{def}	=	mean velocity defect associated with upstream component wake
V_0	=	wake magnitude coefficient
x/M	=	distance downstream from turbulence generation grid nondimensionalized by grid mesh spacing
δ, δ_v	=	propeller wake half-width
θ	=	circumferential position
Λ	=	classic turbulence integral length scale
Φ_{ii}	=	turbulence spectrum in ith direction
ω	=	gust or event frequency ($= 2\pi f$)

Received 14 May 2003; revision received 14 January 2005; accepted for publication 14 January 2005.

*Acoustic Engineer, Code 7250, Hydroacoustics, Carderock Division.
†Chief Scientist, Code 7051, Hydroacoustics, Carderock Division.
‡Roth-Gibson Professor, Department of Aerospace and Mechanical Engineering. Fellow AIAA.

I. Introduction

THE combination of a rotating and stationary set of blades in close streamwise proximity to one another has been used extensively in a variety of applications. The most obvious use relates specifically to a propulsion system (or part of a propulsion system), as with a jet engine. Often, a rotating set of blades used for propulsion is mounted near a stationary structural or steering system, as with a propeller mounted on an aircraft wing, or propeller and rudder mounted on the aft end of a ship. The close proximity of these components translates into a strong influence upon the response of each component to the incoming flowfield.

This influence between rotating and stationary components is often grouped into a fairly broad category called rotor/stator or stator/rotor interactions. The difference between the two categories is simply the streamwise order of the components. [For the purpose of the following discussion, the rotor (propeller) is considered the upstream component and the stator the downstream component, but the lessons learned could be applied to the reverse.] The flow is often dramatically altered by the upstream blade row, and the unsteady loading on the downstream blade row, responding to this modified flowfield, generates an unsteady pressure field, which can radiate sound to the far field. This acoustic output caused by rotor/stator interaction is often quite strong. Therefore, gaining a better understanding of the mechanisms that cause such acoustic output is an important area of research.

One must also consider the fact that these rotor/stator combinations often operate in an environment in which the oncoming flow is already quite turbulent. In a jet engine, the rotor/stator stages of a compressor ingest large vortical structures associated with the wakes of other aircraft and wind gusts. On a ship, propellers and rudders at the stern operate downstream of a hull, which generates highly turbulent flow. This turbulent flow also contributes to the acoustic output of the system by giving an unsteady loading to both the rotor and stator. The unsteady loading on the upstream component complicates the flow for the downstream component in the form of a well-defined wake generated by the response of the upstream component to the ingested turbulence, combined with the normal viscous wake of the upstream component. These effects, as well as the broadband unsteady flow field ingested by the system and modified by the upstream blade row, provide a much different turbulent flowfield for the downstream blade row than its upstream counterpart.

Consider the schematic shown in Fig. 1. Figure 1a shows the flow/acoustic path (or path by which the turbulent flowfield contributes to the acoustic radiation of the system) of a system consisting of a propeller only. The same paths would be present for any aerodynamic body and are not exclusive to a propeller. In any event, the propeller encounters and ingests a turbulent inflow, and, depending on the characteristics of the propeller and ingested turbulence the aeroacoustic response of the system can include both tonal and broadband components. This type of system has been studied using several different approaches as part of the continuing research program at the University of Notre Dame.[1–5] With measurement techniques and models established for this type of system, attention turns to a more complex system involving multiple components.

The flow/acoustic paths for the propeller/stator system are shown in Fig. 1b. In addition to the paths involving the propeller alone (which are still relevant but not presented here for clarity), it is quickly evident that the paths contributing to the stator acoustic output are significantly more involved. The propeller can contribute hub or tip effects as well as wake contributions, but also can modify the turbulence ingested by the system. Further, if the propeller and stator are in extremely close proximity (less than a chord length of the upstream component),[6–8] the unsteady surface-pressure field of each component will have a strong influence on the response of its compliment.

An understanding of the various contributions to this complex flowfield was a primary goal of a larger experimental study of the aeroacoustic response of a downstream blade row. The attempt was made to establish a causal relationship between the influences and their relative contributions. A logical argument can be raised as to the utility of such an endeavor. After all, these influences combine to form a turbulent flowfield, and that total flowfield is responsible for the aeroacoustic response of the downstream component. Models already exist that accurately predict acoustic output based on a defined turbulent inflow. However, if models and techniques can be developed that deconstruct the total flowfield into the sum of its contributions, then these models can be used to individually predict the turbulence levels over a broad scope of problems. Depending on the situation, one or more of these influences might not be present, or might dominate relative to other contributions. If predictive techniques existed that could determine the level of turbulence contributions from each influence based on simple parameters, they would strongly enhance the ability to understand the causes of acoustic radiation and design systems to alter radiation levels.

This paper and its complement[9] begin this effort by distinguishing between turbulence ingested by the system and modified by the propeller and the turbulence contribution of the wake. The wake itself is a combination of a standard viscous wake and the well-defined wake stemming from the propeller's aerodynamic response to its turbulent flowfield. These wake components were selected to be examined first because they have the most general applicability. That is, effects such as hub/tip influences might or might not be present as a result of system geometry, but a body in a real fluid will always have a wake, and real systems will most likely operate in a turbulent environment.

Consider the schematic of Fig. 2a. This represents a typical circumferentially averaged turbulence spectrum downstream of a propeller measured by a probe in the stationary reference frame. In

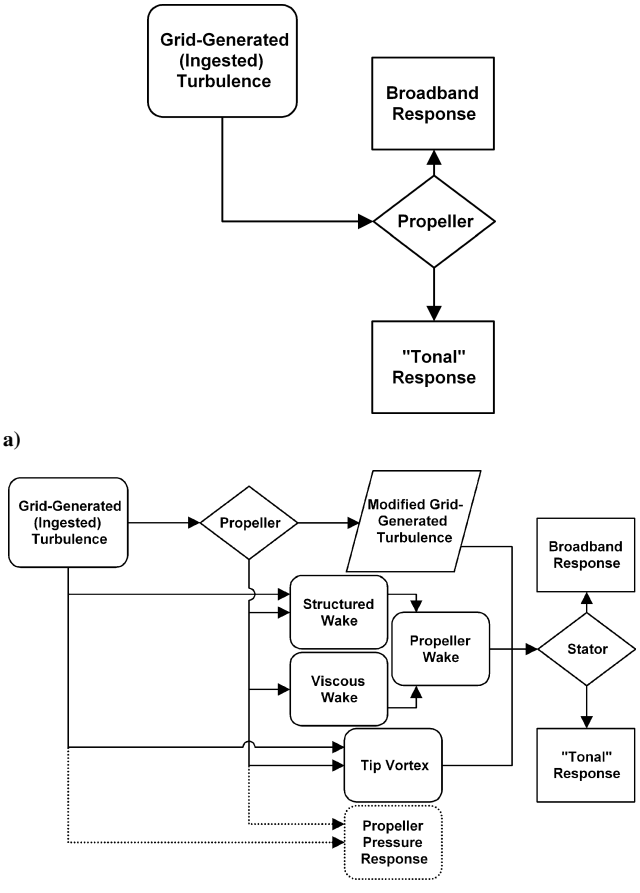

Fig. 1 Flow/acoustic paths of system composed of a) propeller only and b) propeller/stator combination.

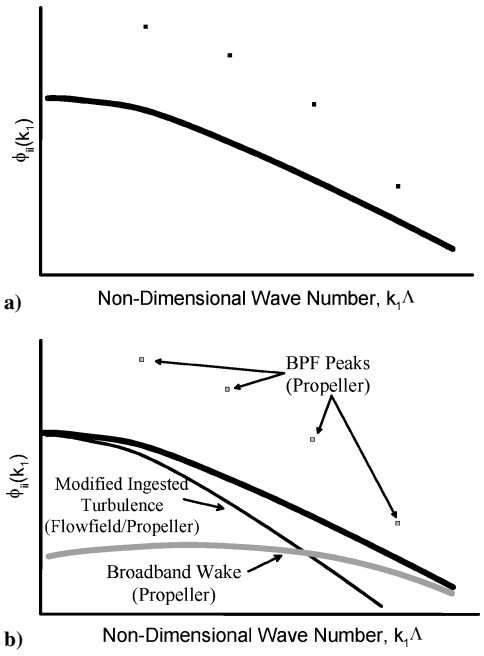

Fig. 2 Schematic of breakdown of typical turbulence spectra downstream of propeller.

other words, this represents the flowfield "seen" by the stator. Typical downstream spectra contain several peaks that occur at much higher levels than the also-present broadband component. Assume that this measurement is outside the region of hub/tip effects and pressure field effects can be neglected. The peaks are obviously caused by the periodic "gusting" caused by the time-mean viscous wakes of the passing propeller blades. However, there is no way to distinguish the broadband contribution of the wake turbulence from that which was ingested and modified by the propeller. If one could isolate the two, the contributions would likely look like Fig. 2b. As the length scales associated with the wake are much smaller than that of the turbulence ingested by the system, there are clear regions of frequency (or convective wave number, with a frozen flow assumption) where one or the other can dominate. Keep in mind that the overall goal of this approach is to deconstruct the information in Fig. 2a to estimate relative contributions, as in Fig. 2b. The balance of this paper focuses specifically on the analysis of the wake contribution to the downstream turbulent flowfield.

II. Background

The study of wake turbulence alone is certainly not new. Rather than present an exhaustive review of such studies, relevant papers that specifically helped in the development of the approach presented here will be mentioned.

As mentioned in Sec. I, the wake of an upstream rotor or propeller is composed of two phenomena superimposed upon one another. The first wake phenomena is associated with normal wake development as would be seen behind any body in a viscous flow. The second phenomena comes from the propeller's response to inflow turbulence. The unsteady pressure field on the propeller blades combines to generate an unsteady lift force on the blades. This corresponds to a change in circulation on the airfoil, resulting in a vortex shed into the wake. Unlike the viscous wake, this wake is highly structured and related to the structure of the turbulence loading the propeller blade. This difference is emphasized in the two papers by Kemp and Sears.[10,11] Because these wake phenomena coexist downstream of the propeller, the distinction between them is somewhat blurred in research efforts because few authors have attempted to separate them. In point of fact, as the wakes are superimposed upon one another, modeling the two separately could prove extremely difficult and be of limited benefit.

An immediate temptation is to characterize this wake considering a comparable single airfoil. Several previous efforts indicate that this would be a mistake. Raj and Lakshminarayana,[12] Satyanarayana,[13] and Majjigi and Gliebe[14] used analytical and experimental techniques to examine the structure of the wake of an airfoil that comprises part of a cascade, concluding it is quite different in structure from a standard airfoil wake. Unlike a standard airfoil, the wake from an airfoil in a cascade is asymmetrical, determined to be caused in part, by airfoil loading. This suggests propeller loading as a possibly significant flow parameter. Further, turbulence intensity levels are significantly higher in the cascade wake, suggesting a strong influence of broadband loading on the downstream stator.

Probably the most extensive experimental study uncovered in terms of characterization of a propeller or rotor wake is that carried out by Inoue and Kuroumaru.[15] A true "brute force" technique, the researchers used a single slanted hot wire to take three-component velocity measurements at 15 radial locations and 70 circumferential sampling points in five measuring planes downstream of the rotor. From this extremely detailed velocity field, derivatives were taken to estimate the vorticity in the flow, as well as examine how these vortical structures decay as they are carried downstream. This detailed an investigation was not something to emulate in the current study. In point of fact, the goal of the current study was to gain a quantitative appreciation of the flowfield through a more simplistic approach involving a minimum of measurements and basic modeling techniques. However, some of the results about the behavior of wake vortical structures are useful in the understanding of the wake behind the propeller in the current study. For example, in terms of relevance to the current unsteady influence being discussed (the propeller wake), results were similar to Raj and Lakshminarayana[12] in that the wake structure was asymmetric immediately downstream of the rotor. However, because of the asymmetric and nonisotropic nature of the turbulence shear stresses resulting from the effect of rotation, the wake becomes symmetrical and two-dimensional as the flow proceeds downstream. Note that although the accurate estimation of turbulent stresses requires the level of detail shown in this study, the simple fact that the wake becomes symmetrical could ease the development of a simple model for the current approach, at least in the limit of appreciable streamwise distance.

III. Experimental Setup

Decomposition of the turbulent flowfield was part of a larger research effort to examine the aeroacoustic response of a stator downstream of a propeller ingesting broadband turbulence. Therefore, an entire series of flowfield, surface-pressure, and far-field acoustic experiments were completed.[16] All experiments were performed in the Anechoic Wind Tunnel (AWT) at the Hessert Center for Aerospace Research at the University of Notre Dame. The AWT was constructed in the early 1990s as part of the development of the Hessert Center for Aerospace Research. The anechoic chamber has a working space 6.1 m (20 ft) wide $\times$ 7.9 m (26 ft) long $\times$ 2.4 m (8 ft) high with 55.9-cm (22-in.) fiberglass sound-absorbing wedges on all six sides. This wedge configuration provides a low-frequency cutoff of about 100 Hz. Above the cutoff frequency, the wedges have a coefficient of energy absorption at normal incidence of 0.99 or greater. A low turbulence subsonic freejet test-section wind tunnel has been developed to fit into this anechoic chamber for aerodynamic and sound-pressure level measurements generated from propellers, fans, pumps, airfoil configurations, etc. The cross-sectional area of the test region is 0.37 m^2 (4 ft^2) with a maximum velocity of about 30.5 m/s (100 ft/s). A complete description of the tunnel's individual components and important characteristics is presented in Mueller et al.[17,18]

A photograph and schematic of the propeller/stator system integrated in the AWT is provided in Fig. 3 and 4, respectively. In the complete case, freestream velocity travels through an upstream turbulence generation grid. Before interaction with a downstream stator, this grid-generated turbulence interacts with a propeller, which both modifies the grid-generated turbulence and generates wake

Fig. 3 Propeller/stator test rig mounted in AWT.

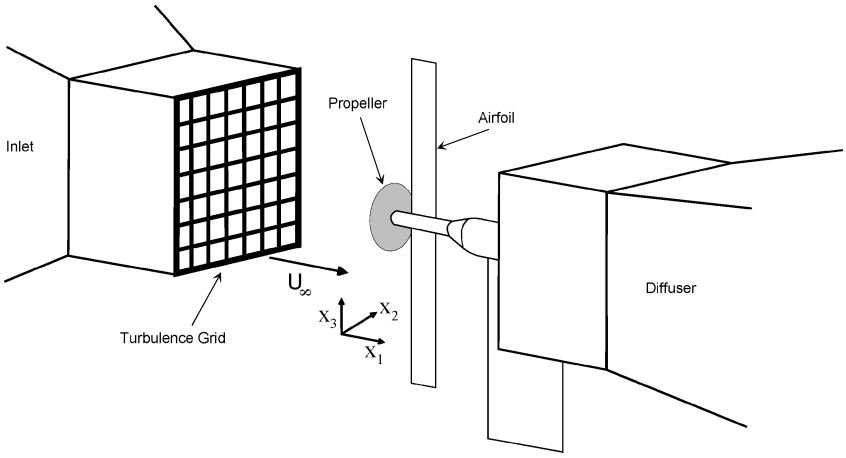

Fig. 4 Experimental setup for airfoil downstream of propeller ingesting broadband turbulence.

Table 1 Key characteristics of turbulence generation grid

Grid parameter	Clean flow	3-in. grid
Mesh size	N/A	7.62 cm (3.0 in.)
Rod diameter	N/A	0.953 cm (0.375 in.)
Grid solidity	0	0.33
RMS turbulence velocity	0.02 m/s (0.07 ft/s)	0.79 m/s (2.60 ft/s)
RMS turbulence intensity	0.15%	6.2%

turbulence of its own. The propeller plane was located 0.61 m (2 ft) downstream of the turbulence generation grids, as the flow has been meticulously examined in this location for both turbulence grid conditions (with and without the presence of an upstream grid). Extensive studies[16,19] have shown that the grid-generated turbulence approaches isotropy in this plane ($x/M = 8$, where x/M is the distance from the grid to propeller plane nondimensionalized by the grid spacing). Key flow characteristics for cases with and without an upstream grid are presented in Table 1.

For the majority of this wake turbulence study, this upstream grid was removed. As the turbulence levels of the empty tunnel were well below that of the propeller-generated turbulence levels, this approach effectively isolated this component of the turbulent flowfield. In the problem of interest, this wake turbulence then convects downstream and over a flat-plate airfoil, an idealized stator. The flat plate used in this study had a constant chord length of 7.62 cm (3 in). The unsteady surface pressure (and thus the far-field acoustics) generated over the stator is the result of the unsteady flow it encounters. The measurement coordinate system for this survey was a standard Cartesian system using primary directions of the flow and airfoil as reference points. For example, the primary (axial) flow direction in the system is represented by x_1. This also represents the chordwise direction of the stator, arranged at 0-deg angle of attack relative to the direction of the freestream flow upstream of the influence of the propeller. Likewise, the normal and spanwise direction of the stator in this orientation are also primary reference directions (x_2 and x_3), respectively.

To examine different parameters associated with the upstream blade row, three different propellers, composed of 4, 10, and 20 blades were used in this study. This was primarily because blade spacing was shown to be critically important to the analysis presented in Part 2 of this paper.[9] However, it also provided an extensive matrix for the analysis of wake turbulence techniques. These propellers are pictured in Fig. 5. The four-bladed propeller has a 25.4-cm (10-in.) diam and a chord length of 6.9 cm (2.4 in.) at a radial position of $0.75R$. The 10-bladed propeller has a 20.3-cm (8-in.) diam and a constant chord length of 2.54 cm (1 in.). Details of these propeller geometries and their performance characteristics can be found in Wojno,[19] Scharpf,[20] and Subramanian.[21] A 20-bladed propeller was simulated by placing two 10-bladed propellers in close axial proximity, with the blades offset by half of the blade spacing relative to the oncoming flow.[16]

Table 2 Summary of experimental operating conditions [freestream velocity 12.7 m/s (41.7 ft/s)]

Propeller	Loading condition	Advance ratio, J	BPF, Hz
4-bladed	Loaded	1.0	200
4-bladed	Unloaded	1.4	142
10-bladed	Loaded	1.14	550
10-bladed	Unloaded	1.31	480
20-bladed	Loaded	1.14	1100
20-bladed	Unloaded	1.31	960

Table 3 Summary of experimental uncertainties

Quantity	Uncertainty, %
Mean velocity	±3.5
RMS turbulence	±5.5
Turbulence autospectrum	±7

An appropriate length scale associated with the positioning of the stator is the maximum chord length of the rotor or propeller blade. At a distance of one chord length, the influence of the unsteady pressure field from either the rotor or stator on its compliment can be ignored.[6–8] Therefore, positioning of the stator (and therefore the location of relevant flow measurements) downstream of the rotor was based on this scaling. The physical spacing in the case of the four-bladed propeller is significantly larger than that of the 10- and 20-bladed propeller because of chord length differences, but preserves the nondimensional spacing of one chord length.

A brief summary of operating conditions is given in Table 2. Operating conditions were selected to take advantage of prior experiments within the same facility.[16,19] Propeller selection was also based on past experience. The rotation rates were based on the desire to have a "loaded" (thrust) and "unloaded" (no thrust) condition for each propeller. However, the range of rotation rate was mechanically limited by the facility's dynamometer, so that even the loaded cases do not represent significant thrust generated by the propeller (coefficient of thrust values for these cases were less than 0.2). The Reynolds number based on propeller chord is on the order of 5×10^5 or larger for all cases considered.

Velocity measurements were taken using an X-wire anemometry probe. The X-wire anemometry probe is able, through proper calibration, to measure two components of the velocity vector simultaneously. By phase-lock triggering data acquisition and manually rotating the probe 90 deg in the probe holder, all three components of the vector could be determined. Careful checking of the measurements in both the x_1-x_2 and x_1-x_3 planes showed excellent matching of the x_1 component (within the experiment's uncertainty for mean velocity measurements; the uncertainty for flow measurements in this study is presented in Table 3), suggesting cross-contamination effects were minimal. For the velocity measurements described here,

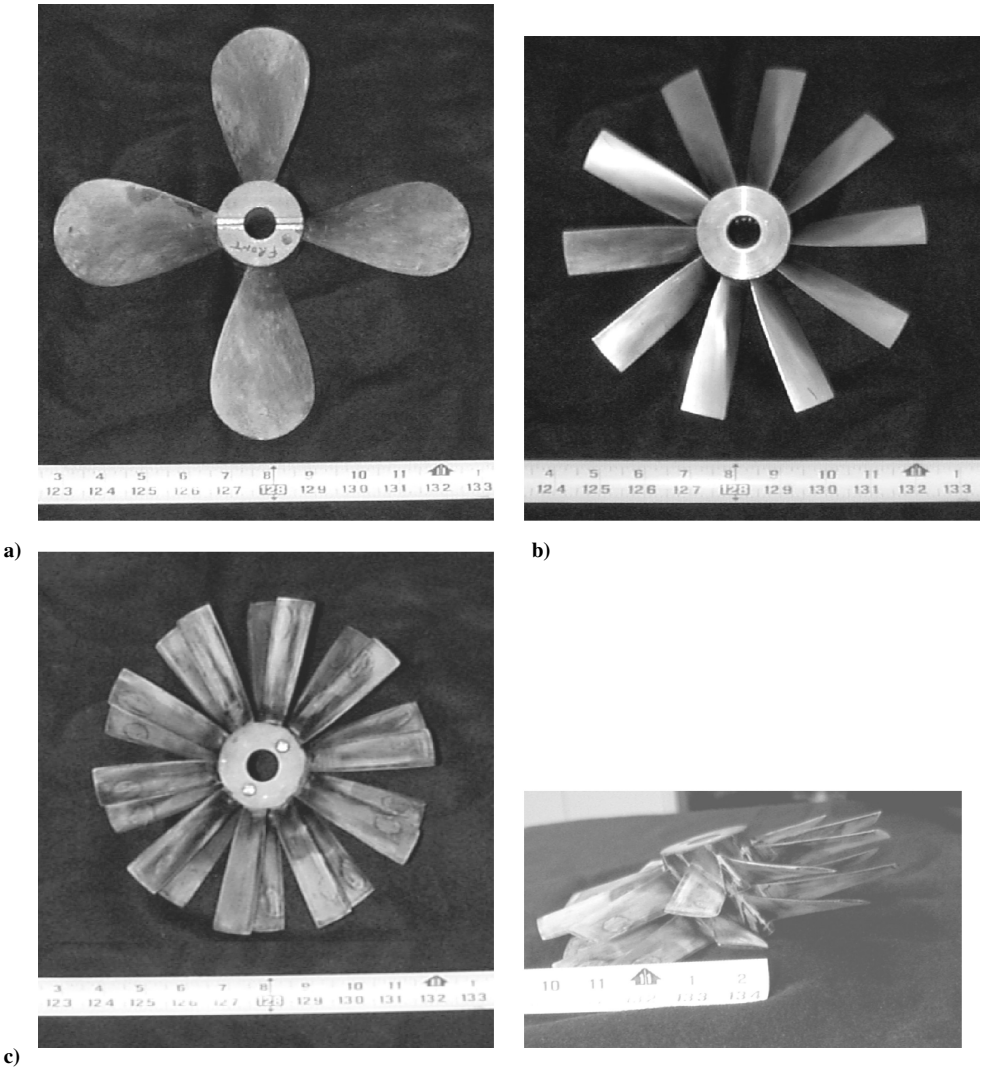

Fig. 5 Photographs of a) 4-bladed, b) 10-bladed, and c) 20-bladed propellers used in current study.

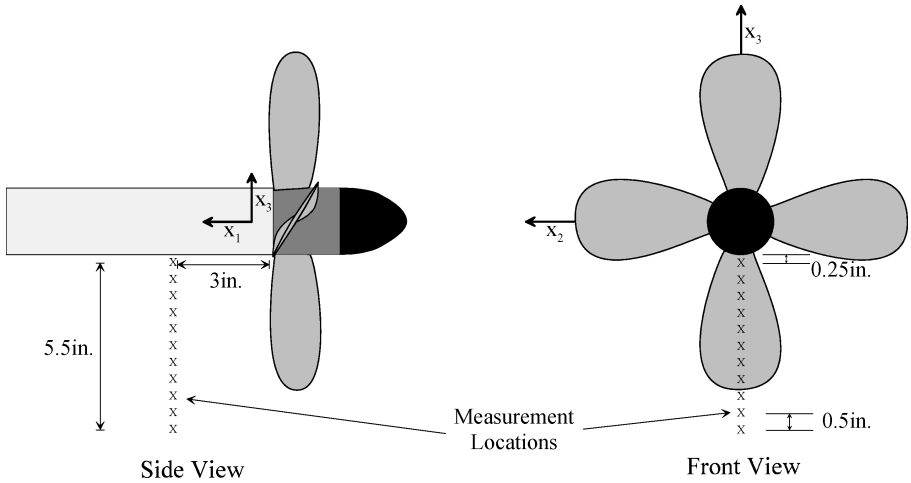

Fig. 6 Schematic of velocity measurement locations (four-bladed propeller locations shown).

both downstream stators were removed, allowing the X-wire probe to be placed at the streamwise location corresponding to the leading edge of the stator. The turbulence characteristics at this point represent the turbulence driving the aeroacoustic response of the stator.

All measurement points involved 625 ensembles of 4096 samples taken at a sampling frequency of 8000 Hz. The locations of the measurements are explained in the schematic in Fig. 6, representing the measurement positions downstream of the four-bladed propeller. The chord length of the 10- and 20-bladed propeller was only 2.54 cm (1 in.), so that the streamwise position of these measurements was much closer to the trailing edge of the respective propellers. All measurements took place beneath the propeller dynamometer shaft and assumed to be equal at matching locations on the top of the dynamometer (top dead center of the propeller plane), which were the locations of the two downstream stator vanes. Geometrical interference from the propeller dynamometer dictated a minimum radial distance from the center of the dynamometer

hub. Therefore, measurements were made in 1.27-cm (0.5-in.) increments starting at a radial distance of 3.18 cm (1.25 in.) from the center of the dynamometer hub and continuing out to a distance of 15.9 cm (6.25 in.) from the center of the dynamometer hub. The outermost distances of each set were considered the freestream condition, as there was no evidence of propeller influence at these locations.

IV. Initial Results

In developing techniques to model the contribution of wake turbulence, efforts focused on the more basic four- and 10-bladed propeller cases. It is beneficial to first examine the raw time- and frequency-domain results. These results give some perspective on the composition of this complex flowfield and provide some justification for the approach taken. With phase-locked triggering of the data sets based on the position of the propeller blades, a time-averaged snapshot of the flowfield can be made at all measurement positions, then marched forward in time. The result is a contour mapping of the flowfield, as shown in Fig. 7 for the case of the four-bladed propeller. Here, there is little to no acceleration of the flow, as the propeller is not loaded. However, there are clear regions (darker areas of the contour) that can be identified with the propeller wake. These wakes pass the measurement plane at nearly the same instant, again consistent with a constant mean flow over the region influenced by the propeller. Also interesting to notice is the region in which tip flow is expected. Although tip vortices are not a part of the current discussion, the contour shading jump, translating into a corresponding velocity jump, at the wake tip region is consistent with the rotation expected with a tip vortex.

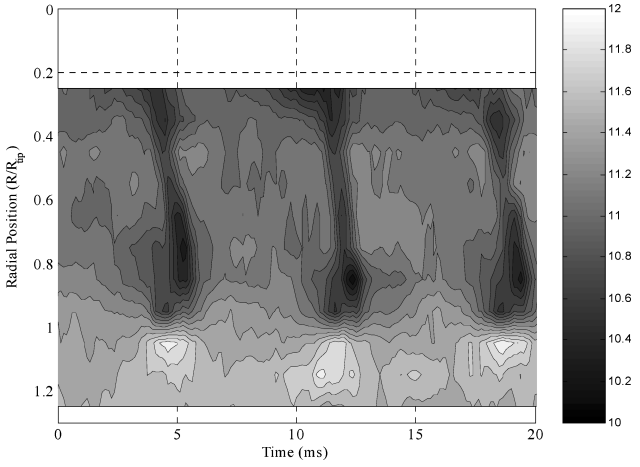

Fig. 7 Phase-locked, time-averaged streamwise velocity downstream of unloaded four-bladed propeller (J = 1.4) (velocity in units of m/s).

At each position and discrete time location, the rms turbulence levels can also be determined. These levels of the normal (x_2-direction) velocity for the same propeller and loading condition are shown in Fig. 8. Recalling that the coordinate system is defined in the reference frame of the stator, this normal component of turbulence defines the "gust" to which the stator responds. Here, it is worthwhile to compare phase-locked rms turbulence levels for cases of the propeller operating in clean flow (Fig. 8a) vs downstream of the turbulence generation grid (Fig. 8b). As with the mean flow plot of Fig. 7, critical structures are plainly obvious in the results. The rms turbulence plots also illustrate a number of key points that will be useful both in the modeling of wake turbulence and isolation of wake and grid-generated contributions.[9] In the absence of an upstream grid, the turbulence is negligible outside of the well-defined propeller wakes. This shows a number of things, at least qualitatively. First, the measurement of wake turbulence alone is possible, as additional tunnel turbulence is effectively zero when compared to wake levels. Also, at least at this downstream location (one propeller chord length in the x_1 direction), the wakes are clearly separable from one another, allowing for a clear definition of appropriate length scales in the wake. Another conclusion can also be made in comparing Figs. 8a and 8b. With clearly defined regions of wake influence, the regions between wakes represent turbulence that is ingested by the system, again suggesting separability. In terms of modeling, this suggests that an approach of superposition of influences might be possible. That is, the total turbulent flowfield can involve the superposition of independent influences. Consider a slice of the rms turbulence level contour plot of Fig. 8b at a radial location 7.0 cm (2.75 in.) from hub center ($R/R_{\text{tip}} = 0.55$). This is shown in Fig. 9. There is little change in the levels associated

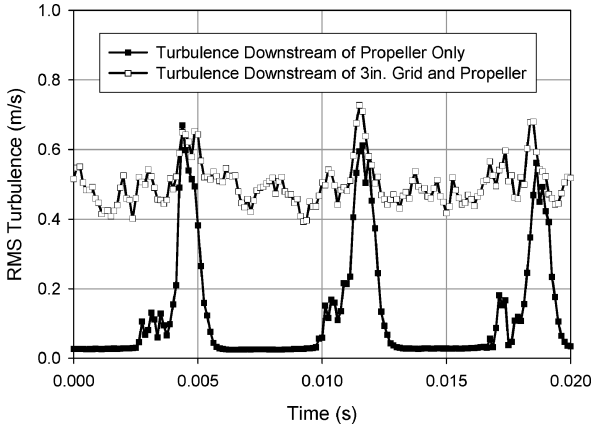

Fig. 9 Phase-locked, time-averaged normal rms turbulence levels downstream of an unloaded four-bladed propeller (J = 1.4) (velocity in units of m/s).

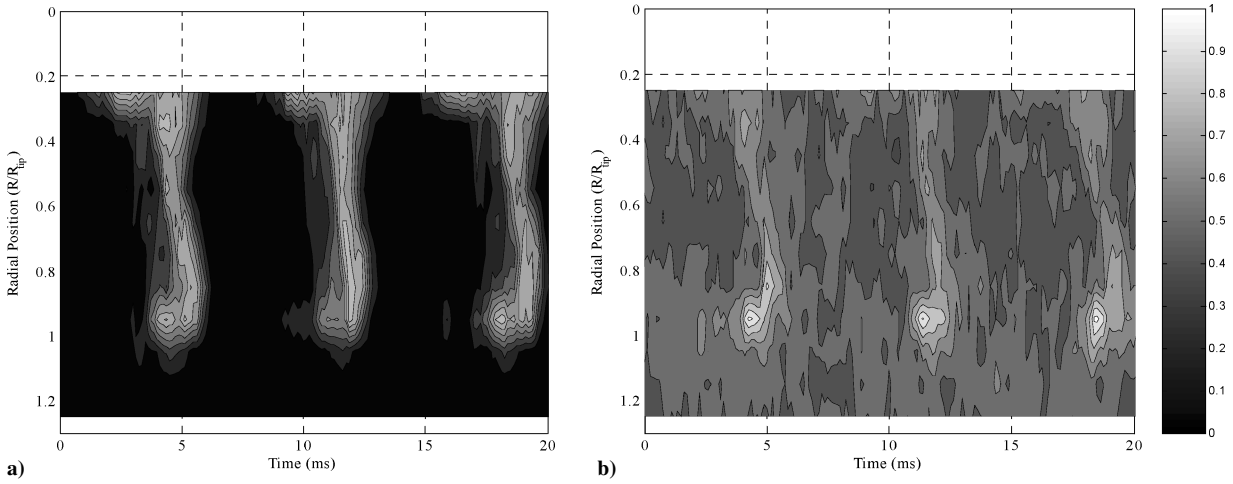

Fig. 8 Phase-locked, time-averaged rms turbulence levels of normal velocity for unloaded four-bladed propeller (J = 1.4) in a) clean flow and b) behind turbulence grid (velocity in units of m/s).

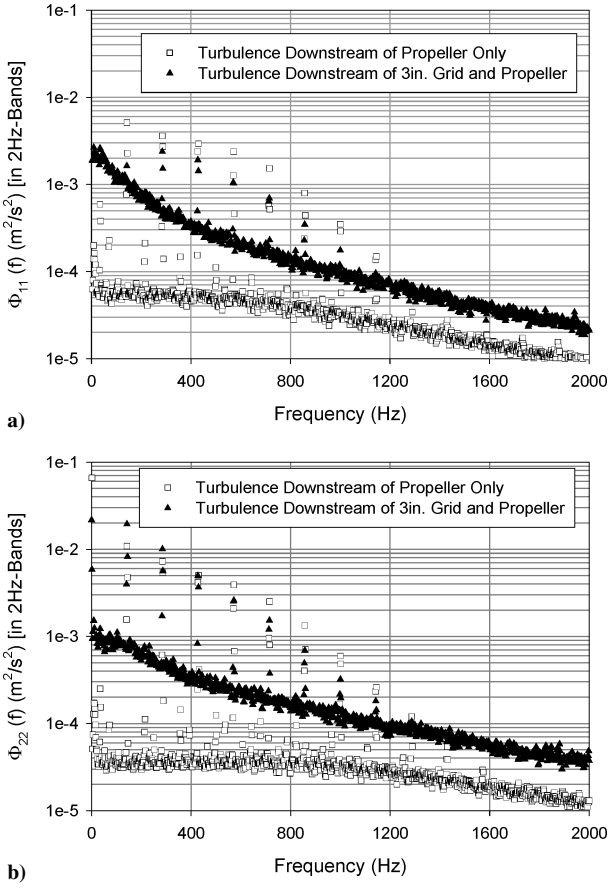

Fig. 10 Turbulence spectra of four-bladed propeller wake at stator leading-edge location, unloaded case ($J = 1.4$), in the a) streamwise and b) normal directions.

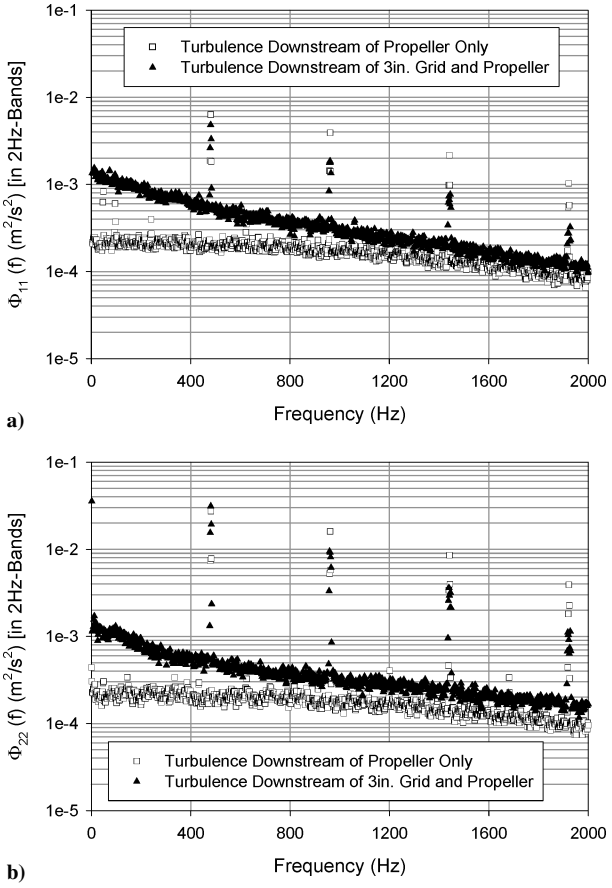

Fig. 11 Turbulence spectra of 10-bladed propeller wake at stator leading-edge location, unloaded case ($J = 1.31$), in the a) streamwise and b) normal directions.

with the propeller wake when comparing cases with and without the upstream grid. However, there is a clear change in the turbulence levels outside of the wake. In the absence of the grid, turbulence levels outside the wake are negligible.

More quantitative conclusions, and the balance of the discussion in this paper, will focus on the spectral domain. These results were converted to the spectral domain via Fourier transform, then ensemble averaged to preserve turbulence information eliminated in the time-averaging technique presented in earlier results. Figure 10 shows the turbulence spectra downstream of the unloaded four-bladed propeller 7.0 cm (2.75 in.) ($R/R_{\text{tip}} = 0.55$) from the hub center. Note that this position is away from hub or tip influences. These results yield a number of important observations that will be useful in the development of modeling techniques. First, the difference between turbulence levels with and without the upstream grid, particularly at low frequencies, closely resembles the discussion in Sec. I. As frequency increases, the contribution of wake turbulence tends to dominate the ingested turbulence levels. As these turbulence spectra represent a circumferential average, increasing the number of blades naturally increases the amount of turbulence associated with the propeller wakes, as seen in comparing the four-bladed propeller case to the identical measurement downstream of the 10-bladed propeller, shown in Fig. 11. In all cases considered, the levels associated with the tonal contribution of the wake do not increase with the presence of ingested turbulence. That is, independent of the inflow condition, the level of gusting associated with wakes passing at blade passage frequency (BPF) is dependent only on the propeller being used.

Outside of a laboratory, the isolation of propeller wake contributions to the total turbulence might not be possible. In such cases, the circumferentially averaged turbulence spectra would resemble the grid and propeller curves in Figs. 10 and 11, namely, a superposition of tonal peaks at BPF and a broadband component, which represents the sum of multiple influences. It is this information that represents the starting point in the isolation of the wake turbulence contribution.

V. Theoretical Model for Wake Turbulence Extraction

From Sec. IV, the turbulence spectra measured by a stationary probe downstream of a propeller record two easily distinguishable phenomena: the broadband turbulence (of multiple influences) and tonal peaks associated with BPF and its harmonics. The BPF peaks are an exclusive feature of the wakes. It is therefore logical to examine this tonal feature to extract information about the wake.

A. Exploiting Tonal Peaks of Periodic Wakes

Before proceeding any further, there exist multiple frames of reference when considering this complex flowfield. Several reference frames can be used, based on the geometry considered. For example, a rotating reference frame would be based on the perspective of the rotating propeller. A stationary frame, the one used in the majority of the discussion of this paper, can follow the geometry of the stator. Finally, a coordinate reference frame can track the streamwise direction of the flow. This reference frame is the most complex, as it can vary with position, and even if uniform flowfield assumptions were made to simplify the situation the true streamwise direction downstream of the propeller would depend on the propeller loading, as this defines the level of the mean swirl component. The point of this discussion is not to generate a robust mapping for moving from one frame to another. Instead, it is to point out that the tools developed here utilize multiple frames of reference, and care must be taken when making comparisons to either return them to one common frame of reference or, if not possible, to at least discuss problems that can be introduced as a result of these differences.

An idea of the physical process involved in the current setup, which will also illustrate issues regarding reference frame, is shown

in Fig. 12. Here, the propeller is unfolded into a cascade, and the blade wakes are convected past a stationary probe. The phase-locked time average of the signal measured by the probe is also shown, and this closely resembles a time "cut" in the contour mapping of Fig. 7. Essentially, there exists a mean flow on that is superimposed a periodic disturbance that represents the wake deficits pictured in Fig. 12.

Now imagine these blade wakes in the rotating reference frame of the propeller itself. In this frame of reference, the blades are stationary, with the wakes convecting downstream from the trailing edge. If a probe were to take a azimuthal cut in space for one revolution as in Fig. 13, the signal measured would be like that of Fig. 14, which is a figure adapted from Chapter 12 of Blake.[6] Here, the wake deficits

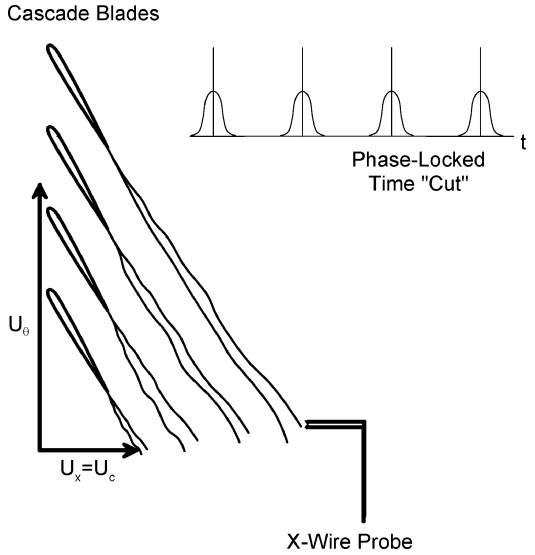

Fig. 12 Schematic of cascade wakes being convected past stationary probe.

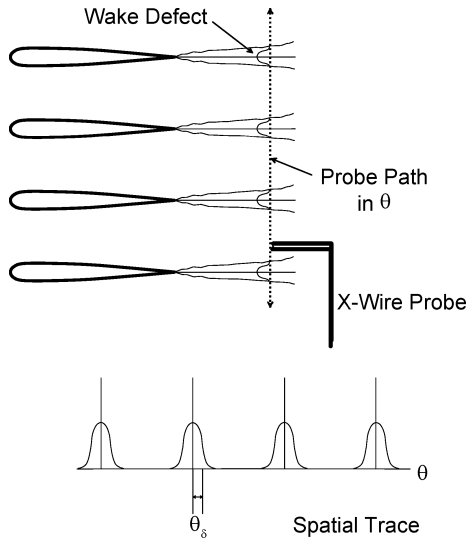

Fig. 13 Schematic of spatial mapping of wake defects.

are modeled as a symmetric decaying exponential of the form

$$U_\infty - U(\theta) = U_{\text{def}} = V_0 e^{-p(\theta-\theta_0)^2} \tag{1}$$

where U_{def} is the velocity defect, V_0 the peak deficit at the center of the assumed symmetric wake centered at azimuthal position θ_0, and p a constant defining the decay rate of the deficit function. The spectral density function $\Phi_{uu_{\text{wake}}}$ of such a mean velocity profile, when plotted as a function of azimuthal wave number k_θ, is a series of tonal peaks located at the harmonics of the number of blades B. The magnitudes of these peaks fit the curve described by the expression

$$\Phi_{uu_{\text{wake}}} = \left(B^2 V_0^2 / 4\pi p\right) e^{-k_\theta^2/2p} \tag{2}$$

It stands to reason, therefore, that an exponential curve fit, of the form presented in Eq. (2), could matched to the tonal peaks of a given turbulence spectrum. Knowing the total number of blades, this fit would then give the constants V_0 and p, thereby providing an approximation to the wake deficit profile.

Returning to the physical measurement outlined in Fig. 12, the wakes are not specifically sampled as already outlined. Assuming the blades are unloaded or lightly loaded, the wakes convect past the probe in the x_1 direction [as defined upstream of the propeller and the reference frame of the stator (see Sec. III)] at the convection velocity. If the rotational velocity of the propeller is the same as the convection velocity, then the wakes are spaced the same way as just defined. However, as shown in Fig. 12, in the event that they are not equal, the space over which the wakes are distributed in this measurement frame is different from the corresponding rotational frame. Therefore, in the stator reference frame, which represents the reference frame of the measurements in this experiment, the spatial distribution is dependent on the wave number k_x. This wave number is related to k_θ as

$$k_x = k_\theta (U_\theta / U_x) = k_\theta (U_\theta / U_\infty) \tag{3}$$

where these velocities are defined, in the stator reference frame, as in Fig. 12. The governing equation, which will utilize this reference frame of the probe, can thus be written

$$\Phi_{uu_{\text{wake}}} = \left(B^2 V_0^2 / 4\pi p\right) e^{-{k_x}^2/2p} \tag{4}$$

where the peaks in the k_x frame are those of the k_θ frame but scaled according to the difference in velocity.

This model was determined assuming a symmetric wake of exponential shape. As mentioned in Sec. II, this assumption, particularly for a loaded propeller, might be inappropriate. Further, the reference frame considered here is not the propeller reference frame, and so the wake might be skewed as a result of the measurement technique. However, following the conclusions of Inoue and Kuroumaru,[15] even the wake of a loaded propeller eventually evolves into a symmetric shape as downstream distance increases. As to the change in reference frame, the time-series results of the current experimental study provide a means of direct comparison with predictions, so that the validity of such a model can be directly examined.

B. Using Wake Shape to Define Broadband Wake Contribution

Now that a basic shape for the propeller wakes has been defined, it is not difficult at all to define classical length scales for the wake.

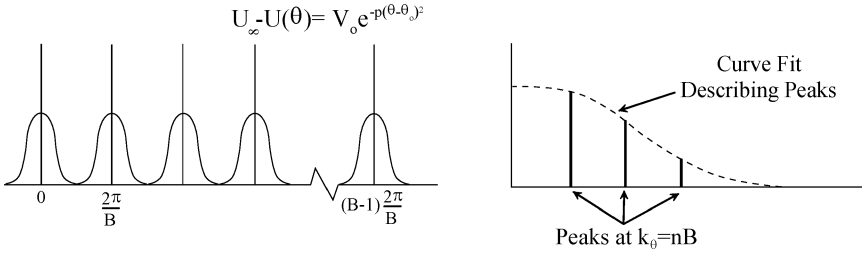

Fig. 14 Schematic of Fourier transform of periodic wake.

These can include momentum thickness, displacement thickness, or wake thickness as defined by the half-width[22] and are simple to compute now that a closed-form solution to describe the shape of the wake has been determined.

Recall from Figs. 7–9 of Sec. IV that the turbulence associated with the wake is concentrated in discrete cuts of the time signal. That is, the turbulence of the wake is clearly concentrated within the wake region itself. Outside of the defined wake, there is clearly no contribution from the wake. This rather obvious notion, however, carries with it a tool for further wake analysis: The width of the wake represents the largest scales associated with the wake turbulence contribution. Put another way, the integral length scale of the wake turbulence, which, in effect, represents the largest eddies of turbulent flow, should be on the order of the wake thickness.

The wake half-width δ is defined as the spatial distance from the maximum defect to the point where the defect is one half of the maximum, as shown in Fig. 13. There are two such distances in any given wake (one to each side), but assuming the wake is symmetric the two are equal to one another. Using the notation of Eq. (1), the half-width can be determined in terms of radians to be

$$[U_\infty - U(\theta)] = V_0 e^{-p(\theta-\theta_0)^2}, \qquad [0.5V_0] = V_0 e^{-p(\theta_\delta)^2}$$

$$\theta_\delta = \sqrt{\ell_n(0.5)/-p} \tag{5}$$

where θ_δ is the half-width in radians. This distance is not a function of wake deficit magnitude V_0 at all, but merely a function of the exponential shape factor p. This can be converted to a physical distance by multiplying by the radial distance of the measurement position from the hub center of the propeller:

$$\delta = \theta_\delta r \tag{6}$$

Note that there is nothing physically special about the half-width except that it has been used as a convenient choice for length scale in the nondimensionalization of wake parameters in the past. It stands to reason, however, that the integral length scale of the broadband contribution of wake turbulence should be on the order of the velocity half-width, $\Lambda \sim \mathcal{O}(\delta)$.

Once the half-width thickness is determined, a prediction for the broadband turbulence of the wake can be made by assuming a curve shape to describe the turbulence. The simplest example (although not necessarily appropriate in all cases) is to use Hinze's result for isotropic turbulence,[23] namely,

$$\Phi_{11}(k_1) = \frac{2\Lambda}{\pi}\frac{1}{1+k_1^2\Lambda^2} \tag{7}$$

$$\Phi_{22}(k_1) = \frac{\Lambda}{\pi}\frac{1+3k_1^2\Lambda^2}{\left(1+k_1^2\Lambda^2\right)^2} \tag{8}$$

where coordinate directions are as defined in Sec. III and all spectra are scaled such that

$$\oint_{-\infty}^{\infty} \Phi_{ii}(k_1)\,\mathrm{d}k_1 = \oint_{-\infty}^{\infty} \Phi_{ii}(\omega)\,\mathrm{d}\omega = 1 \tag{9}$$

Thus, the overall methodology for determining the wake contribution to the overall turbulence spectra is defined. The procedure is summarized next:

1) The tonal peaks are a result of a periodic gusting of the mean flow caused by the wake contribution. An exponential for the wake profile is assumed, resulting in a curve describing the magnitude of the tonal peaks. Using spectra determined experimentally, the constants for wake magnitude and shape can be determined.

2) Once a wake profile shape has been determined, all classic wake length scale parameters can be determined as necessary.

3) The maximum length scales of turbulence are defined using the classic turbulence integral length scale. It stands to reason, therefore, that the scale of the wake width is on the same order as the integral length scale of the turbulence.

4) Using the integral length scale assumed to be on the order of the wake width, a prediction for the broadband turbulence contribution of the wake can be made by assuming a curve shape for the relative levels of the turbulence spectrum.

This analysis implied a number of additional assumptions, which are not crucial in the development of the technique but help to simplify the approach dramatically. The validity of such assumptions must be examined as part of the overall assessment of the technique. These will be the topic of discussion in Sec. IV. The primary assumptions include the following:

1) An exponential curve fit was assumed for the wake defect. This model depends not only on an assumption of wake symmetry, but also that the wakes can be easily distinguished from one another. That is, the adjacent wakes do not overlap one another in the temporal/spatial domain.

2) The integral length scale of the wake turbulence is of the order of the thickness of the wake, $\Lambda \sim \mathcal{O}(\delta)$.

3) A curve fit is assumed for the broadband contribution of the wake, based on the integral length scale of the turbulence. In this case, the curves represent those anticipated in an isotropic condition. It is obvious that the global flowfield downstream of the propeller is nonisotropic. However, the local turbulence within the propeller wake itself can evolve to resemble an isotropic state as it convects downstream. It must be emphasized that the assumption of an isotropic curve is not primary to the theory of extracting this broadband wake information. Rather, it is more beneficial to more global applications if the broadband levels can be inferred assuming one length scale, whether an isotropic curve is used to describe the broadband turbulence or not.

VI. Analysis of Wake Extraction Technique

The following sections summarize an analysis of the assumptions used in and results of the wake extraction technique outlined in Sec. V. The techniques were applied to the entire matrix of propellers and loading conditions at appropriate downstream measurement flow locations. The results presented here focus on one measurement location for all flowfield conditions: a radial location of 7.0 cm (2.75 in.) ($R/R_{\text{tip}} = 0.55$) from the propeller hub center at a streamwise distance from the propeller of one propeller chord length. The entire matrix is not presented here, both for brevity and so the implementation of the technique can be clearly demonstrated. Again, results are discussed in terms of the frame of reference of the stator.

A. Analysis of Isotropic Turbulence Curve Assumption

Although not of primary interest to the current investigation, the assumption of an isotropic curve to describe the broadband wake turbulence contribution does merit some examination. As stated in Sec. V.B, the more important result would be the ability to represent the broadband contribution with a single, easily determined length scale. However, it is worthwhile to examine if such a curve would accurately represent the wake turbulence at this downstream location, as the wake should approach this condition as it evolves downstream.

To examine the isotropic curve assumption, the turbulence spectra from the case without an upstream turbulence grid were examined. The peaks associated with blade passage, an artifact of change between the rotating and stationary reference frames, were artificially removed, leaving only the broadband turbulence component caused by the propeller wakes. Using Taylor's hypothesis of frozen flow, frequency was converted to convective wave number assuming freestream velocity in the x_1 direction only. When properly nondimensionalized, the integral length scale can be determined from Eq. (7) in the limit as the nondimensional wave number $k_1\Lambda \to 0$. These experimental values will be discussed further in Sec. VI.C. Equations (7) and (8) can then be used to generate isotropic curves for comparison with experimental results.

Typical results are shown in Figs. 15 and 16, and similar results were present for all propellers and loading conditions considered. The excellent agreement between the theoretical and experimental curves (within the experimental uncertainty of 7%) for both

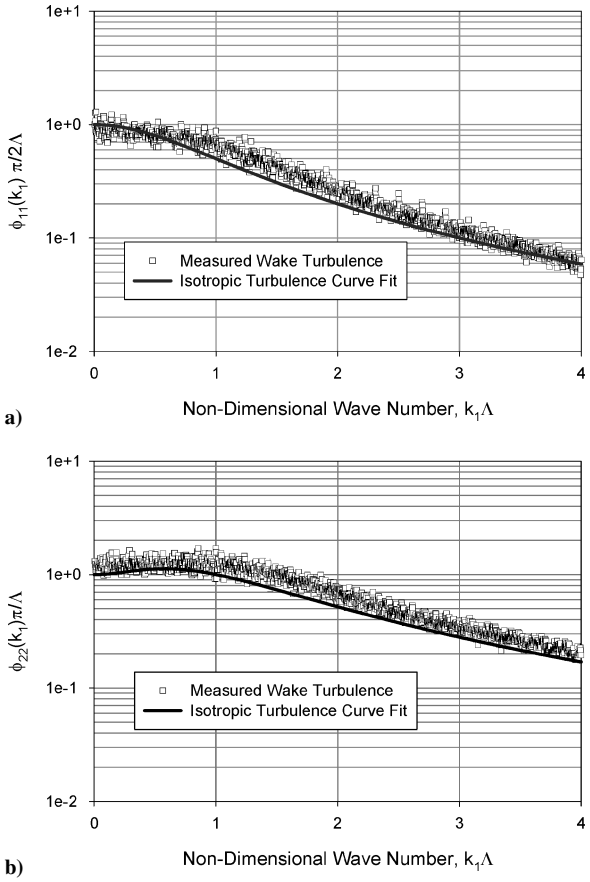

Fig. 15 Propeller wake isotropy check for four-bladed propeller at stator leading-edge location, unloaded case ($J = 1.4$), in the a) streamwise and b) normal directions.

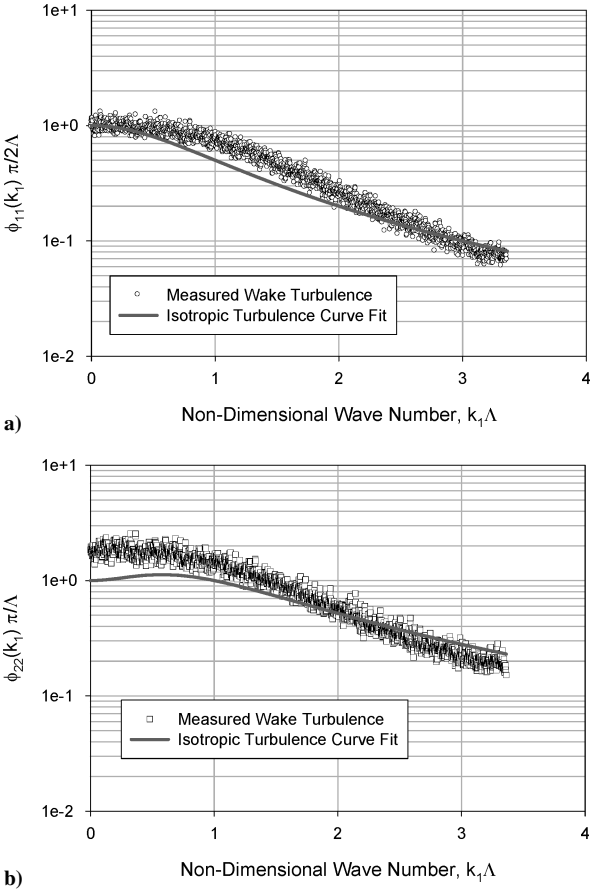

Fig. 16 Propeller wake isotropy check for 10-bladed propeller at stator leading-edge location, unloaded case ($J = 1.31$), in the a) streamwise and b) normal directions.

streamwise and normal directions gives the indication that, with the proper integral length scale, this length scale, rms wake turbulence levels, and the isotropic curve assumption are enough to completely characterize the broadband wake contribution of the turbulence. (The rms turbulence levels of the wake are needed in the nondimensionalization process, but represent a scaling constant that can be easily determined experimentally.) The most important conclusion is, however, that a single length scale, as yet undetermined using the wake extraction methods of this paper, can be used to predict broadband turbulence levels for the spectra in multiple coordinate directions.

B. Reconstruction of Periodic Mean Flow

Beginning with the turbulence spectra similar to those shown in Figs. 10 and 11, the first process in extracting wake turbulence contribution information is to fit a curve describing the magnitude of the tonal peaks according to the equations of Sec. V.A. The resulting mean flow pattern is plotted against the phase-locked, time-averaged results obtained by making a cut in the appropriate contour plots (like Fig. 17) and scaled to match the analysis techniques.

Typical results are shown in Fig. 17. For both the unloaded four- and 10-bladed propeller cases, the technique appears to overpredict the magnitude of the wake deficit, and, to a lesser extent, underpredict the width of the wake. From Eq. (5), the difference in magnitude is not important to the current effort. However, this difference is still somewhat disconcerting. Rather than a flaw in the technique, it is believed that these differences are the result of the difference in the averaging technique used. The experimentally determined time series is phase-locked averaged in the time domain, whereas the wake reconstruction is the result of a data set ensemble averaged in the frequency domain. When averaged in the temporal domain, small changes in the rotational speed (a dithering of the propeller rotation) have a "dulling" effect on the wake of the time-averaged signal. That is, the time-averaged signal has a lower, wider profile shape than the single data sets that compose it. This effect is not as significant in the spectral domain. This is because the small changes in rotational speed, manifested in a change in frequency, do not exceed the bin width of the Fourier transform. Therefore, though the rotational frequency changed, the energy associated with the wake gust is still captured in the same frequency bin.

An illustration of this phenomena is shown in Fig. 18, which shows the time-averaged signal used to construct the contour plot of Fig. 7 at a radial location of 7.0 cm (2.75 in.) ($R/R_{\text{tip}} = 0.55$). In the contour plot, the signal was limited to that part of the time signal associated, roughly, with the first rotation of the propeller. As the data are triggered on a fixed point of propeller rotation, the effects of small differences in rotational speed are minimized in this part of the time-averaged signal. However, as acquisition time increases to the end of the data set, the small differences have a profound effect on the signal. If this effect were not present, the peaks associated with wake defects at the end of the time-averaged signal would be similar in magnitude and width to those at the beginning of the signal. This is because the blades creating the defect are the same, operating in the same flow conditions. This effect is discussed in detailed in Appendix A of Minniti.[24]

Returning to the current discussion of Fig. 17, the part of the signal least influenced by this averaging error is used for the comparison. However, this effect is still present, is difficult to quantify, and is likely the cause of the discrepancy between the theoretical curve of the wake extraction technique and the experimental results.

C. Using Turbulence Extraction Methods to Predict Wake Integral Length Scale

To this point, this paper has outlined a means to predict the mean flow variation associated with periodic wake disturbances, as well as established the possibility of using a single length scale for the

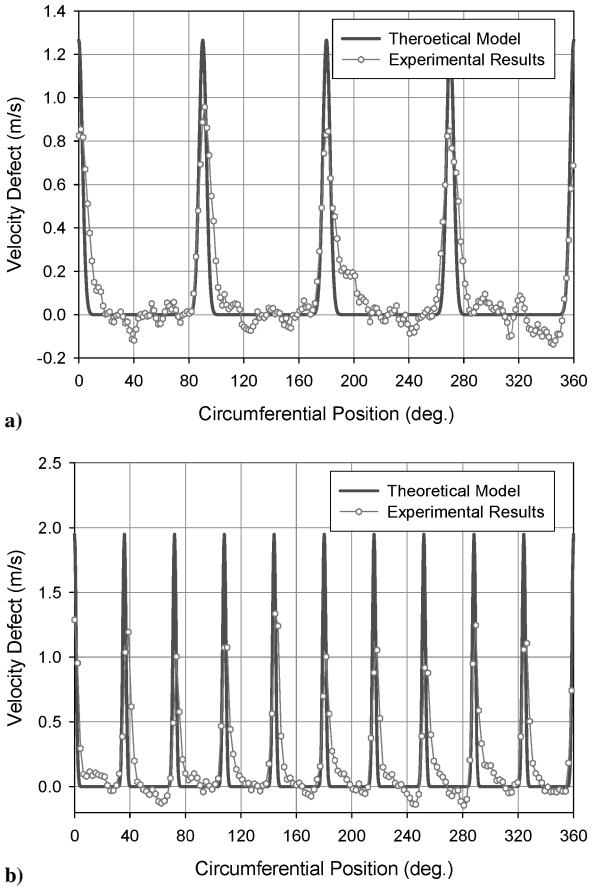

Fig. 17 Comparison of phase-locked, time-averaged mean velocity patterns in streamwise direction for unloaded a) 4- and b) 10-bladed propeller.

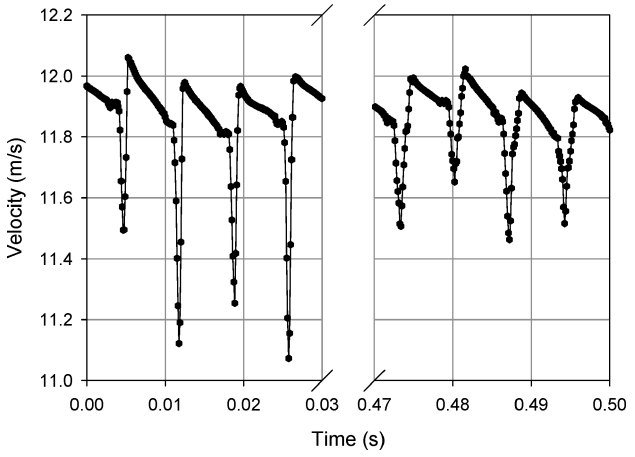

Fig. 18 Illustration of the effect of small differences in propeller rotational velocity on phase-locked, time-averaged signal (four-bladed propeller, $J = 1.4$).

estimation of the broadband wake turbulence contribution. The next step involves using the calculated mean flow profile to estimate the integral length scale of the turbulence on physical grounds.

As pointed out in Sec.V.A, reference frame differences have the potential of seriously influencing the effectiveness of this technique. Some steps were taken to properly map the results in the reference frame of the experimental data. Still, the definition of streamwise direction is not the true direction of the mean flow. This is primarily because of the swirl complexity introduced by the propeller. Therefore, instead of focusing the analysis of length scale estimation on the streamwise direction (as defined in the reference frame of the stator) only, a similar approach was made using the spectral results of the normal direction. Using the same approach as outlined in Sec. V.B. for the streamwise direction, a second length scale for each flowfield condition δ_v is calculated based on the turbulence spectra of the normal direction. Again, the goal is to ensure the technique is more globally applicable and not strongly dependent on the exact resolution of true streamwise direction. In the case where the rotational velocity is much greater than the stator's streamwise component of velocity, $U_\theta \gg U_x$ (see Fig. 12), the classical definition of the wake defect, shown in Fig. 13, is more closely represented by the stator's normal component of velocity.

Table 4 Comparison of measured integral length scale and half-width of unloaded propeller wakes

Propeller/loading condition	Λ, cm	δ, cm	δ_v, cm
4-bladed, unloaded	0.30	0.33	0.37
10-bladed, unloaded	0.17	0.15	0.16
20-bladed, unloaded	0.19	0.16	0.17

Table 4 shows the result for all propellers in the unloaded condition for the measurement location considered. The column labeled as the integral length scale Λ represents the turbulence integral length scale as calculated using the method outlined in Sec. VI.A, and can be viewed as the appropriate length scale choice for characterizing the broadband wake turbulence contribution. In all cases considered, δ and δ_v, defined based on Eq. (6) and differing only in the component of velocity used, are consistent with one another, translating into the possibility of relaxation of the streamwise direction in defining the wake profile shape. The widths of the 10- and 20-bladed propellers are nearly identical, as they should be considering the blades are the same geometry. Further, rather fortuitously, the wake half-widths very closely resemble the integral length scale of the wake turbulence in all cases.

There is nothing particularly remarkable or special about the selection of the velocity half-width as the length scale of choice. The idea was put forward that the length scale of wake turbulence was on the order of the width of the wake. This is usually many times larger than the momentum or displacement thickness of a wake.[22] Therefore, the half-width was selected for its use as a scaling quantity in other wake studies, as well as the knowledge that it was certainly on the order of the width of the wake. There was no real physical significance behind its selection over other scales on the same order. The only concept was an order of magnitude argument; that is, $\Lambda \sim \mathcal{O}(\delta)$. The fact that this particular choice of length scales closely matched the necessary length scale for the isotropic curve mapping is encouraging, but there is nothing more significant than repeatability for the entire, albeit limited, matrix of run conditions considered here to suggest that such a length scale might be more globally applicable. The most important conclusion is that the integral length scale and wake width are of the same order.

D. Influence of Propeller Loading

Propeller loading is an area requiring more examination. The test matrix here was defined by the mechanical limitations of the facility (mainly the rotation rate of the propeller dynamometer). As a result, the maximum loading achievable with the propellers considered was still quite small. In fact, the 10-bladed propeller (which also is used to construct the 20-bladed propeller, as discussed in Sec. III) is essentially a research propeller designed to provide small blade spacing, and so little loading is possible simply because of the geometry. When the theory for extracting wake turbulence information was applied to these 10- and 20-bladed cases, the resulting wake half-width again matched the integral length scale of the turbulence, as shown in Table 5. The case with the most loading in the matrix is the loaded, four-bladed case. This loading is a more realistic load condition for actual applications. This case also had the most significant departure from the expected value of Λ, particularly in the calculation of the length scale δ_v. This is particularly disturbing when considering the point made in Sec. VI.C that the stator's normal component of velocity should more accurately capture the classic wake defect shape, especially with increased loading (caused by an increase in U_θ).

Table 5 Comparison of measured integral length scale and half-width of loaded propeller wakes

Propeller/loading condition	Λ, cm	δ, cm	δ_v, cm
4-bladed, loaded	0.32	0.27	0.70
10-bladed, loaded	0.17	0.17	0.20
20-bladed, loaded	0.19	0.21	0.20

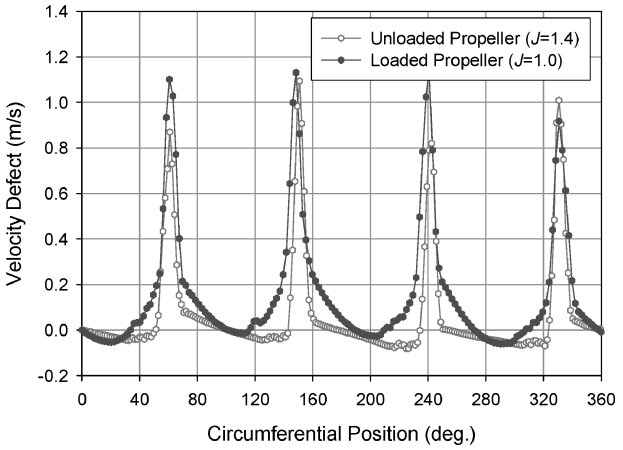

Fig. 19 Comparison of phase-locked, time-averaged wake shapes for normal component of velocity downstream of four-bladed propeller.

There are not enough data to conclude that loading is the significant factor in these small discrepancies. However, it does merit further investigation. First, in looking at Tables 4 and 5, the experimentally determined value for Λ has not changed significantly. Therefore, there must be something in the technique itself that is causing such a discrepancy. Consider Fig. 19, which compares the phase-locked, time-averaged signals of the normal component of velocity for the loaded and unloaded four-bladed propeller cases. Although the distribution would obviously be different in the temporal domain, when rescaled in the circumferential spatial domain, the center points of the wakes are roughly aligned.

One quickly notices that the basic shape of the wake is similar. In point of fact, the half-widths of the wake, or distances between the centerline of the wake and point on either side where the defect is half of the magnitude at the centerline, are essentially the same. Because the unloaded case δ_v matches both loaded and unloaded values of the experimentally determined Λ, and from Fig. 19 appears to match the half-width of the loaded case, the prediction of the loaded case should be essentially equal. Yet when this value is calculated using the curve fit of the spectral peaks, the result is a significant increase in δ_v. The answer is suggested in closer examination of the loaded propeller wake shape. Although the distance from centerline to half-width is nearly identical, the wake shape from the half-width point to the freestream is substantially increased. This bell-shaped widening of the wake profile suggests a substantially larger contribution to the profile is contained in the lowest blade passage harmonics.

As an exercise, the technique was reapplied to both the unloaded and loaded four-bladed propeller conditions, first employing all harmonics seen above the broadband levels in the turbulence spectrum, then removing the lowest harmonics from consideration (to the extent that such an approach was possible given the limited number of data points above the broadband). These peaks were simply removed as data points to the curve fit. Thus, the curve fit was simply weighted to emphasize the higher harmonic data points. The influence of such weighting on δ_v is summarized in Table 6, whereas the influence on the shape of the calculated wake profile is shown in Fig. 20. These results suggest that ignoring the data points of the lowest harmonics for the loaded case results in the same superb predictive capability of the technique that was seen in the unloaded cases. Further, the unloaded case is basically unaffected if the same approach is taken. This suggests that, for the unloaded condition, the data points of the lower harmonics match the curve fit involving only the data from the upper harmonics.

Table 6 Comparison of calculated half-widths δ_v resulting from suppression of low blade passage harmonic data points in four-bladed propeller loaded and unloaded cases

Blade passage harmonics used	Loaded case δ_v, cm	Unloaded case δ_v, cm
All	0.70	0.37
All but 1st	0.42	0.36
All but 1st–2nd	0.42	0.35
All but 1st–3rd	0.38	N/A
All but 1st–4th	0.37	N/A
All but 1st–5th	0.36	N/A

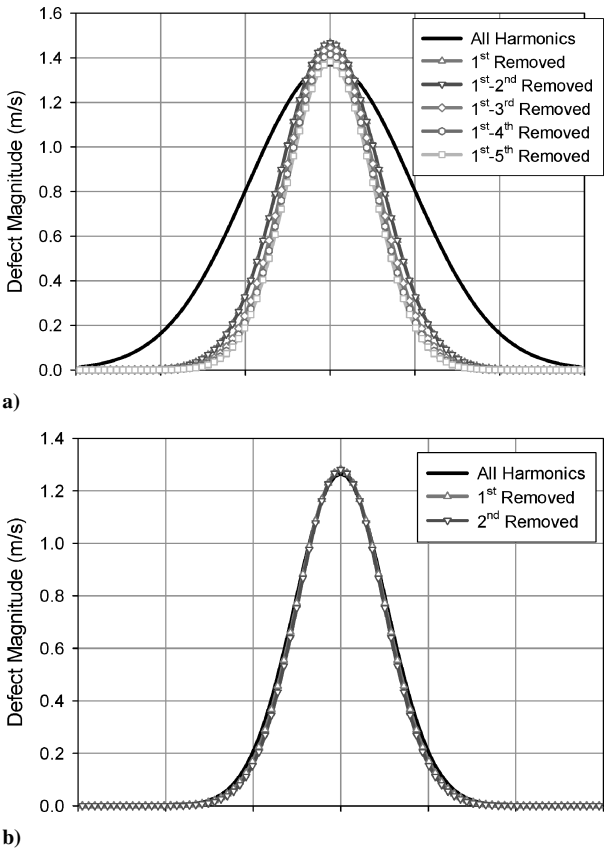

Fig. 20 Comparison of wake defect profile shapes by removal of lower harmonic dependence for a) loaded and b) unloaded four-bladed propeller.

Although these results are encouraging, the test matrix studied simply does not provide enough data for the cases of loaded propellers. From the limited amount that was included, results suggest that loading the propeller can increase the complexity of the system in a way not accounted for in the approach outlined in Sec. V. Still, results continue to support the original hypothesis that the turbulence integral length scale is of the order of the wake thickness, and (from Sec. VI.A) this length scale and an isotropic turbulence assumption do an excellent job of predicting the broadband levels of the wake turbulence contribution. This result holds significant promise in the modeling of complex flows in that a simple approach does an excellent job of capturing the relevant physics of the flowfield.

E. Concerns with Wake Turbulence Extraction Technique

In looking at the results of this study, it would be easy to conclude that a universal technique for extracting wake turbulence contributions is presented. Although this is true for all cases considered, the complexity of the system presents areas of concern. These concerns need to be addressed in future tests. It is hoped that this paper lays the groundwork for establishing a theory that is truly universally applicable, both in terms of the theory presented and in terms of the areas where further research is certainly warranted.

One area is concern is the influence of propeller loading, as explained in Sec. VI.D. Another area of concern must be the streamwise evolution of turbulence. The theories developed in this paper stem from experimental results at one downstream location. Of course, this location was dependent on propeller chord length, so it varied for different cases in the test matrix. Many rotor/stator applications involve a separation on the order of a chord length, and these results can be beneficial for such cases. However, in cases of separation much less than or much greater than a chord length, this approach might be less effective. For cases involving less separation, the assumption of local isotropy of the wake turbulence is certainly less likely, and the wake will most likely be asymmetric. Therefore, an alternate model will likely be required, though the concept of a single length scale might still be applicable. Further downstream, a propeller wake will continue to spread to the point of interacting with adjacent wakes. This interaction can adversely affect the results of this approach, but certainly the spreading of the wakes will cause a decrease in the peak levels associated with BPF. At some point, the peaks might be indistinguishable from the broadband levels, which would correspond to a loss of the periodic mean flow behavior seen here and represent the downstream limitation of such an extraction method. In any event, it is worthwhile to further examine the influence of wake evolution on this technique.

The results presented in this paper represent an important, detailed first step in the concept of separating broadband turbulence influences in a flow regime such as this. These additional considerations are not presented to throw doubt on the techniques developed so much as to identify areas of concern when extending these techniques beyond the test matrix considered. It is hoped that this paper and its compliment[9] represent the first step of development of a unified theory for isolation and reconstruction of broadband turbulent sources in a highly complex environment such as the one considered.

VII. Conclusions

This paper sought to introduce and develop a theory for the isolation and evaluation of wake turbulence to the complex flowfield downstream of a propeller. As tonal peaks associated with blade passage frequency are a contribution to the flowfield exclusive to the propeller wake, these peaks were used to infer a time-averaged shape to the wake profiles. As turbulence associated with the wake is concentrated in the borders of the wake itself, its contour helps to define critical length scales for describing the broadband turbulence.

The integral length scale of the wake turbulence, a term synonymous with the largest eddies of turbulence, was assumed to be on the order of the wake thickness. A useful length scale of the same order is the velocity profile's half-width, which is often used in the nondimensional characterization of wake development. Results from the test matrix considered show that this length scale is also an accurate prediction of the integral length scale of the flow, and that this scale can then be used to accurately predict the broadband contribution of the wake turbulence levels.

Looking to extend this theory for more universal application, a number of primary issues, as yet unresolved, are also discussed. It is hoped that the methodology and resulting issues presented in this paper will lead to further examination beyond the limitations of the current experimental setup, such that the techniques can be improved and strengthened as other variables are considered in more detail.

This paper and its complement[9] represent a foothold in the overall goal of a unified approach to distinguish between sources contributing to the complex flowfield downstream of one component of a propeller/stator system. If these sources can be distinguished from one another, it holds promise for identifying and addressing the sources that contribute to the aeroacoustic response of a downstream aerodynamic body.

Acknowledgments

This research was performed at the Hessert Center for Aerospace Research of the Department of Aerospace and Mechanical Engineering at the University of Notre Dame. The work was supported by the U.S. Navy, Office of Naval Research, located in Arlington, Virginia, under Contracts N00014-99-1-0284 and N00014-01-1-0424. The Program Manager was L. Patrick Purtell.

References

[1]Minniti, R. J., III, and Mueller, T. J., "Experimental Investigation of Unsteady Aerodynamics and Aeroacoustics of a Thin Airfoil," *AIAA Journal*, Vol. 36, No. 7, 1998, pp. 1149–1156.

[2]Minniti, R. J., III, Blake, W. K., and Mueller, T. J., "Inferring Propeller Inflow and Radiation from Near-Field Response, Part 1: Analytic Development," *AIAA Journal*, Vol. 39, No. 6, 2001, pp. 1030–1036.

[3]Minniti, R. J., III, Blake, W. K., and Mueller, T. J., "Inferring Propeller Inflow and Radiation from Near-Field Response, Part 2: Empirical Application," *AIAA Journal*, Vol. 39, No. 6, 2001, pp. 1037–1046.

[4]Wojno, J. P., Mueller, T. J., and Blake, W. K., "Rotor Turbulence Ingestion Noise, Part I: Experimental Characterization of Grid-Generated Turbulence," *AIAA Journal*, Vol. 40, No. 1, 2002, pp. 16–25.

[5]Wojno, J. P., Mueller, T. J., and Blake, W. K., "Rotor Turbulence Ingestion Noise, Part II: Rotor Aeroacoustic Response," *AIAA Journal*, Vol. 40, No. 1, 2002, pp. 26–32.

[6]Blake, W. K., *Mechanics of Flow Induced Sound and Vibration*, Wiley, New York, 1986, Chaps. 11 and 12.

[7]Kaji, S., and Okazaki, T., "Generation of Sound by Rotor-Stator Interaction," *Journal of Sound and Vibration*, Vol. 13, No. 3, 1970, pp. 281–307.

[8]Falk, E. A., "An Experimental Investigation of Aerodynamic Forcing in the F109 Turbofan Engine Compressor," Ph.D. Dissertation, Dept. of Aerospace and Mechanical Engineering, Univ. of Notre Dame, Notre Dame, IN, 2000.

[9]Lynch, D. A., III, Blake, W. K., and Mueller, T. J., "Turbulent Flow Downstream of a Propeller, Part 2: Ingested, Propeller-Modified Turbulence," *AIAA Journal*, Vol. 43, No. 6, 2005, pp. 1211–1220.

[10]Kemp, N. H., and Sears, W. R., "Aerodynamic Interference Between Moving Blade Rows," *Journal of the Aeronautical Sciences*, Vol. 20, No. 9, 1953, pp. 585–597, 612.

[11]Kemp, N. H., and Sears, W. R., "Unsteady Forces due to Viscous Wakes in Turbomachines," *Journal of the Aeronautical Sciences*, Vol. 22, July 1955, pp. 478–483.

[12]Raj, R., and Lakshminarayana, B., "Characteristics of the Wake Behind a Cascade of Airfoils," *Journal of Fluid Mechanics*, Vol. 61, No. 4, 1973, pp. 707–730.

[13]Satyanarayana, B., "Unsteady Wake Measurements of Airfoils and Cascades," *AIAA Journal*, Vol. 15, No. 5, 1977, pp. 613–618.

[14]Majjigi, R. K., and Gliebe, P. R., "Development of a Rotor Wake/Vortex Model," NASA TR 174849, June 1984.

[15]Inoue, M., and Kuroumaru, M., "Three-Dimensional Structure and Decay of Vortices Behind an Axial Flow Rotating Blade Row," *Journal of Engineering for Gas Turbines and Power*, Vol. 106, July 1984, pp. 561–569.

[16]Lynch, D. A., III, "An Experimental Investigation of the Unsteady Response of a Stator Located Downstream of a Propeller Ingesting Broadband Turbulence," Ph.D. Dissertation, Dept. of Aerospace and Mechanical Engineering, Univ. of Notre Dame, Notre Dame, IN, 2001.

[17]Mueller, T. J., Scharpf, D. F., Batill, S. M., Strebinger, R. B., Sullivan, C. J., and Subramanian, S., "The Design of a Low-Noise, Low-Turbulence Wind Tunnel for Acoustic Measurements," AIAA Paper 92-3883, July 1992.

[18]Mueller, T. J., Scharpf, D. F., Batill, S. M., Strebinger, R. B., Sullivan, C. J., and Subramanian, S., "A New Low Speed Wind Tunnel for Acoustic Measurements," *Proceedings of the European Forum on Wind Tunnels and Wind Tunnel Test Techniques*, Royal Aeronautical Society, London, 1992.

[19]Wojno, J. P., "An Experimental Investigation of the Aeroacoustic Response of a Ten-Bladed Rotor Ingesting Grid-Generated Turbulence," Ph.D. Dissertation, Dept. of Aerospace and Mechanical Engineering, Univ. of Notre Dame, Notre Dame, IN, 1999.

[20]Scharpf, D. F., "An Experimental Investigation of the Sources of Propeller Noise due to Turbulence Ingestion," Ph.D. Dissertation, Dept. of Aerospace and Mechanical Engineering, Univ. of Notre Dame, Notre Dame, IN, 1993.

[21]Subraminian, S., "Experimental and Computational Studies on Propeller Noise Due to Inflow Distortion," Ph.D. Dissertation, Dept. of Aerospace and Mechanical Engineering, Univ. of Notre Dame, Notre Dame, IN, 1993.

[22]Schlichting, H., *Boundary Layer Theory*, McGraw–Hill, New York, 1979.

[23]Hinze, J. O., *Turbulence*, McGraw–Hill, New York, 1975.

[24]Minniti, R. J., III, "An Experimental Investigation of Thin Airfoils Exposed to Periodic Gusting Including the Inverse Aeroacoustic Problem," Ph.D. Dissertation, Dept. of Aerospace and Mechanical Engineering, Univ. of Notre Dame, Notre Dame, IN, 1997.

W. Devenport
Associate Editor